Identification and quantification of soundscape components in the Marginal Ice Zone

Florian Geyer,[a] Hanne Sagen, Gaute Hope, and Mohamed Babiker
Nansen Environmental and Remote Sensing Center, Bergen, Norway

Peter F. Worcester
Scripps Institution of Oceanography, University of California San Diego, La Jolla 92093-0225, California, USA

(Received 27 October 2015; revised 14 March 2016; accepted 28 March 2016; published online 15 April 2016)

Acoustic experiments using an integrated ice station were carried out during August 2012 and September 2013 in the Marginal Ice Zone (MIZ) of Fram Strait. The two experiments lasted four days each and collected under-ice acoustic recordings together with wave-in-ice and meteorological data. Synthetic aperture radar satellite data provided information on regional ice conditions. Four major components of the under-ice soundscape were identified: ship cavitation noise, seismic airgun noise, marine mammal vocalizations, and natural background noise. Ship cavitation noise was connected to heavy icebreaking. It dominated the soundscape at times, with noise levels (NLs) 100 km from the icebreaker increased by 10–28 dB. Seismic airgun noise that originated from seismic surveys more than 800 km away was present during 117 out of 188 observation hours. It increased NLs at 20–120 Hz by 2–6 dB. Marine mammal vocalizations were a minor influence on measured NLs, but their prevalence shows the biological importance of the MIZ. The 10th percentile of the noise distributions was used to identify the ambient background noise. Background NLs above 100 Hz differed by 12 dB between the two experiments, presumably due to variations in natural noise sources.
[http://dx.doi.org/10.1121/1.4945989]

[JFL] Pages: 1873–1885

I. INTRODUCTION

The focus of this paper is to study the soundscape of the Marginal Ice Zone (MIZ) of Fram Strait, located between Greenland and Svalbard. This strait is the only deep-water connection between the world oceans and the Arctic Basin. The circulation pattern is dominated by the transport of warm water into the Arctic along the Svalbard side and the transport of cold water southward from the Arctic on the Greenland side (e.g., de Steur *et al.*, 2014). The circulation causes the eastern side of the strait to be ice-free ocean, while the western side of the strait is more or less covered with southward drifting ice. The MIZ is the transition zone between the ice covered portion of Fram Strait and open ocean. The ice conditions in the MIZ range from diffuse ice to compact ice, newly frozen grease ice to multiyear ice, and floe sizes from a few meters to hundreds of meters. The wind, wave and mesoscale processes along the ice edge determine the location, configuration, and composition of the MIZ (e.g., Johannessen *et al.*, 2003). These processes are natural sound generation mechanisms in the MIZ, which therefore has a different soundscape compared to the interior Arctic.

Ambient noise levels (NLs) in the interior Arctic are generally low and characterized by episodic sound generating mechanisms, such as ridging, break up of sea ice, and thermal cracking (e.g., Makris and Dyer, 1986; Pritchard, 1990; Lewis and Denner, 1988). Recent investigations, however, indicate that a large part of the Arctic ice cover has become seasonal, much more dynamic, and exposed to atmospheric influence (e.g., Kinda, 2013). Therefore, the future Arctic soundscape can be expected to have characteristics similar to those previously observed in the MIZ.

In the MIZ the primary natural sound-generating mechanisms are due to ocean processes impacting the sea ice dynamics, such as ocean waves propagating into the ice pack, ice edge eddies, inertial oscillations, and internal waves generated at the ice edge (Makris and Dyer, 1991; Lynch *et al.*, 1993; Johannessen *et al.*, 2003). The temporal variations in sound generation are significant in the MIZ, driven by the direction of wind and waves relative to the ice edge. During on-ice wind and wave conditions, the sea ice is compact, and a large number of sound generating mechanisms create a more or less continuous high background sound level in the MIZ (e.g., Sagen, 1998; Johannessen *et al.*, 2003). During off-ice wind and wave conditions and low sea state, the sound level has been observed to be significantly lower with 10–15 dB differences at frequencies above 100 Hz (e.g., Johannessen *et al.*, 2003; Sagen *et al.*, 2014). Considerable spatial variability in ambient NL depending on the distance from the ice edge and on the concentration of sea ice were observed in previous studies (e.g., Makris and Dyer, 1991; Johannessen *et al.*, 2003; Sagen *et al.*, 2014). The sound level is particularly low in areas with grease ice, which

[a]Electronic mail: florian.geyer@nersc.no

dampens sound generating waves at the sea surface (Johannessen *et al.*, 1994).

The MIZ is an area with high biological productivity during spring and summer, and this attracts fish and marine mammals. Analysis of a yearlong recording (2008–2009) from a passive listening system at 79°N in the western part of Fram Strait showed that seasonal variability in vocalization varies from species to species. Bowhead whale calls are heard year round. Blue whales are heard from June to October, while fin whale calls are heard from August to March (Moore *et al.*, 2012; Klinck *et al.*, 2012).

The MIZ is more exposed to acoustic noise generated by human activities like shipping, icebreaker operations, and seismic air guns than the interior Arctic. Recordings in Fram Strait and the Greenland Sea have shown that most of the year signals from seismic airguns dominate the low frequency portion of the soundscape (Moore *et al.*, 2012; Klinck *et al.*, 2012). In Fram Strait this is mostly not nearby activity. Sound from airguns used 1400 km away at the coast of Norway is heard in Fram Strait. As the sound reaches the ice edge, it is attenuated with distance into the ice pack (Tollefsen and Sagen, 2014). Human activities, such as icebreaker operations, commercial shipping, and air guns used for seismic exploration, are increasing in Arctic and sub-Arctic areas. This will change the composition of the soundscape in the Arctic and in particular, in the MIZ. It is therefore important to establish the baseline and the natural variability of the sound levels to be able to quantify human influence.

In this paper we analyze data from a drifting integrated ice station (IIS), which collected four days of continuous acoustic recordings each in 2012 and in 2013 as part of the Waves-in-Ice Forecasting for Arctic Operators (WIFAR) project. The aim was to investigate the relation between environmental conditions and ambient noise, as well as the acoustic fingerprint of selected human activities: icebreaker operations and seismic exploration. This study concentrates on identifying and quantifying four main components of the observed soundscape: seismic airgun noise, ship cavitation noise during heavy icebreaking maneuvers, marine mammal vocalizations, and natural background noise during quiet periods of the recordings. Section II presents the experimental setup, describes the environmental conditions, and gives an overview of the acoustic recordings. Sections III–VI focus on the individual soundscape components. A comparison of their strength and prevalence concludes the article in Sec. VII.

II. EXPERIMENT DESCRIPTION

Two field experiments, in August 2012 and September 2013, were carried out as part of the WIFAR project in the Fram Strait MIZ. In both experiments an IIS was deployed and drifted for four days before it was recovered. The IIS continuously recorded acoustic and environmental conditions as observed from an individual ice floe drifting with the ice field. Along with the *in situ* observations, high-resolution remote sensing data were collected to monitor ice conditions. This section describes the instrumentation and the data sets collected in the two experiments.

A. Instrumentation and data processing

The IIS consisted of (1) an under-ice acoustic array consisting of 2–4 self-contained hydrophone modules, (2) a meteorological station, and (3) a wave-in-ice buoy that contained a three-axis accelerometer. All surface modules had GPS positioning. The meteorological station measured temperature, wind speed and wind direction at 1 m and 5 m above surface. The recordings of the under-ice acoustic array were stored internally in each hydrophone.

The hydrophones used were High Tech, Inc. HTI-90-U. These hydrophones are nominally rated for 2 Hz to 20 kHz, but our units have a high-pass filter at 10 Hz to reduce strum. In addition, the hydrophone module input has a high-pass filter at 7.7 Hz. The instrument sample rate was 3906.25 Hz.

Spectrograms were calculated from calibrated and detrended acoustic pressure data using 50% overlapping Kaiser windows with a length of 1024 samples to produce time series of power spectrum density (PSD). This results in a spectrogram consisting of one spectrum every 0.131 s (corresponding to a sample rate of 7.63 Hz). The frequency resolution of the resulting spectra is 3.81 Hz. The high temporal sampling enables us to observe rapidly varying components of the noise field. To observe the low frequency component, we increase the length of the Kaiser windows to 16 384 samples, still with 50% overlap. This increases the frequency resolution to 0.24 Hz, but on the other side this leads to one spectrogram each 2.10 s. This corresponds to a sample rate of 0.48 Hz for the time series at a chosen sound frequency.

Seven satellite images from Radarsat2 were acquired during the experiments, four images in 2012 and three images in 2013. The images are in Scansar wide mode covering an area 500 km wide with 100 m resolution and dual polarization HH /HV. The images were mainly used for deployment and tracking of the instrument, studying ice conditions, and mapping the ice edge.

B. Setup and environmental conditions in the 2012 experiment

The IIS was deployed on a medium-sized floe at 1200 UTC on 25 August 2012. The floe was roughly 200 m by 50 m in size, 1.5–3 m thick, and located at 79° 40′N, 001° 49′E, about 6 km from the ice edge. After four days, the ship returned to the ice flow and the IIS was recovered at 79° 28′N, 000° 2.34′E. The hydrophone modules were clamped to the wire 19 m and 21 m below the surface. The hydrophone at 19 m depth is used in this study.

The satellite image in Fig. 1(a) is from the day of deployment of the ice station. Lines indicate the changes in ice edge position on consecutive days until the recovery of the IIS. This indicates that on-ice wind and wave conditions pushed the ice edge in a north-westerly direction, leading to a general compression of the ice field during the first three days and some decompression (relaxation of the ice field) on the fourth day. The track of the drifting IIS is plotted with dots on top of the satellite image, using the same shades as for the ice edge. The distance from the IIS to the ice edge decreased from 6.0 km on 25 August 2012 to 5.2 km on 27 August 2012 and then increased again to 6.3 km on 29

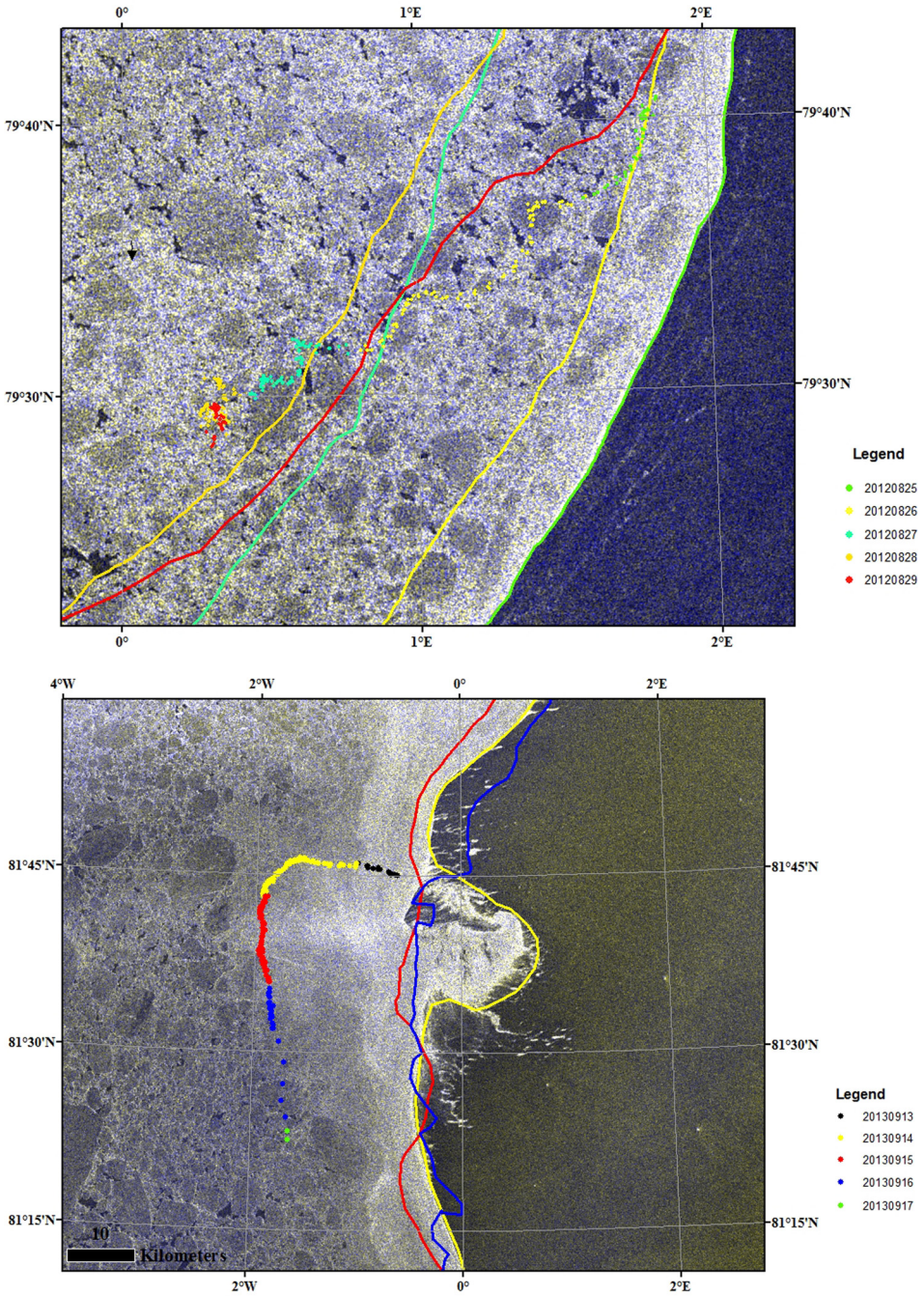

FIG. 1. (Color online) (a) Radarsat2 synthetic aperture radar (SAR) satellite image depicting ice conditions and the drift of the IIS during the 2012 experiment. The satellite image was acquired on 25 August 2012, the day when the IIS was deployed. The position of the ice edge for each day of the experiment is marked by solid lines. The drift of the ice buoy from northeast to southwest (25–29 August 2012) is marked by dots in identical shades as the ice edge markings. (b) SAR satellite image depicting ice conditions and the drift of the IIS during the 2013 experiment. The satellite image is acquired on 14 September 2013, the second day of the IIS deployment. The drift of the ice buoy from northeast to southwest (13–17 September 2013) is marked by dots. SAR satellite images are available for three days during the deployment to determine the position of the ice edge: 14, 15, and 16 September 2013, the line shadings are identical to the ice buoy drift markings.

August 2012. The trajectory shows a southwesterly drift of the IIS with the distinct signature of inertial oscillations. The amplitude of the inertial oscillations decreased towards the end of the IIS drift, likely because of the increased compression of the ice field combined with reduced wind speed. A summary of the environmental conditions during the deployment period is presented in Table I.

C. Setup and environmental conditions in the 2013 experiment

The IIS was deployed 20 km from the ice edge on an ice floe that was approximately 1.5 m thick and 50 m by 50 m in area. The deployment took place on 13 September 2013 at 81° 45′N, 001° 49′W and recovery was done four days later at 81° 20′N, 001° 42′W. Four hydrophone modules were clamped to a 33 m long wire at depths of 15, 20, 25, and 30 m. The uppermost hydrophone at 15 m depth is mainly used in this study. Background NLs from all four hydrophones are compared in Sec. VII.

Figure 1(b) displays a satellite image from the day of deployment of the IIS with lines denoting the changes in the ice edge position on consecutive days. The satellite data show a stable north-south oriented ice edge. The distance from the IIS to the ice edge varied from 18.7 km (14 September 2013) to 24.8 km (15 September 2013) before decreasing again to 20.8 km (16 September 2013). A summary of the environmental conditions during the deployment period is presented in Table I.

TABLE I. Summary of environmental conditions for the 2012 and 2013 experiments.

Environmental parameter	WIFAR 2012 experiment			WIFAR 2013 experiment		
Date	25.8.	26.8.	27.8.–29.8.	13.9.–14.9.	15.9.	16.9.–17.9.
Wind [m/s]	5–8	8–10	2–5	10	0	2–4
Wind direction	—[a]			East (along ice-edge)		
Significant wave height [m]	0.25–1.5	1–1.9	<1	0.75–1.2	0.75–1.2	0.25
Dominant wave period [s]	15–17 s	15–17 s	15–17 s	12	14	14
Ice conditions	Compact ice, ice compression during deployment period			Close, broken up ice between station and ice edge		

[a]Not available due to instrument error (movement of ice edge indicates on-ice wind direction).

D. Acoustic observations

Figures 2 and 3 present the four-day long acoustic recordings obtained during the two experiments. The two recordings show strong variability in NLs and types of observed noises in the frequency range (8–1950 Hz).

The 2012 recording (Fig. 2) is dominated by cable strumming noise at frequencies below 20 Hz, which is identifiable by the sharp maximum at 9 Hz. The second dominant noise component is the distant seismic airgun noise observed from 25 to 100 Hz during large parts of the recording. Other noise components are ship engine noise at 330 Hz, ship noises from icebreaking (10–50 Hz), marine mammal vocalizations (80–200 Hz), and transient noise events from direct hydrophone contacts. Examples of each of these noise types are annotated in Fig. 2.

The noise observed in the 2013 experiment (Fig. 3, upper panel) differs sharply from the observations in the previous year. Nearly half of the recording is dominated by very strong noise from ship propeller cavitation during heavy icebreaking activity of the research vessel (see Roth *et al.*, 2013, for a thorough discussion of propeller cavitation from icebreaking vessels). In the top panel of Fig. 3, four different time periods are denoted A–D. During periods A and C the ship cavitation noise dominates the frequency range from 8 to 1950 Hz, with characteristic maxima (strong spectral lines) at 30, 75, 90, 400, and 800 Hz. In periods B and D ship cavitation noise is only occasionally observed. During period A (hours 19–37), ship cavitation noise occurs with the icebreaker close by. During period C (hours 68–88), the icebreaker is 70–130 km from the ice station (Fig. 3, lower panel). During the quiet periods B (hours 40–67) and D (hours 89–111), ship engine noise is observed as a distinct line in the spectrogram at 330 Hz. Seismic airgun noise is present from 20 to 100 Hz and is an important component of noise variability during the periods without cavitation noise. The signals at 900 Hz are from an acoustic communication experiment carried out in parallel with the acoustic recording (Freitag, 2015).

Some of the main soundscape components can be identified in NL distributions of the 2012 and 2013 experiments (Fig. 4). In 2012 strumming noise dominates all percentiles at 8–12 Hz (Fig. 4, left panel). Also, ship engine noise is identifiable as sharp spectral peaks at 300, 670, and 1000 Hz. During extraordinary ship maneuvering captured in the higher percentiles, the number of spectral peaks due to ship engine noise increases. Seismic airgun noise and noise from marine mammal vocalizations contribute to the difference between high and low percentiles of the NL distribution at 20–500 Hz, but they are not easily identifiable as they increase NLs over a wide spectral range. Broad spectral peaks at 17, 34, 65–70, and 110 Hz at the highest percentile levels are connected to icebreaking activity of the research vessel. They are similar to the ship cavitation noise observed in the 2013 experiment, but much weaker.

The NL distribution of the 2013 experiment (Fig. 4, right panel) is dominated by strong noise from ship

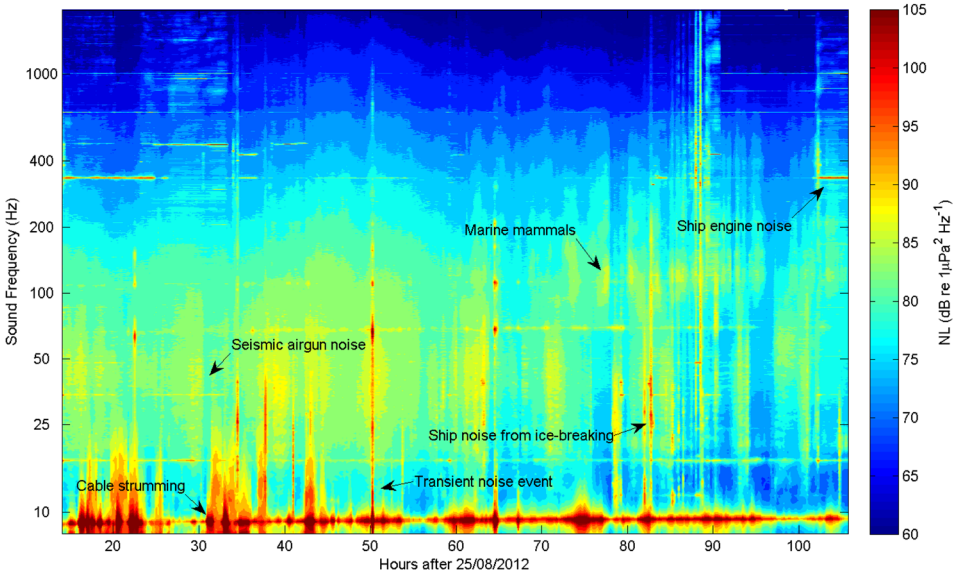

FIG. 2. (Color online) Overview of passive acoustic recording in the 2012 experiment: spectrogram of 15-min mean acoustic NLs (NLs) with 0.24 Hz frequency resolution. The main different sound types visible are ice breaking noise (12–50 Hz), seismic exploration noise (20–120 Hz, maximum at 40 Hz), marine mammal vocalizations (80–500 Hz, maximum at 120 Hz) and ship engine noise (horizontal lines at 330 Hz and various higher frequencies). Increased NLs at hours 50 and 64 are due to hydrophone hits; increased noise at hours 87–89 is due to ship extraordinary ship maneuvering.

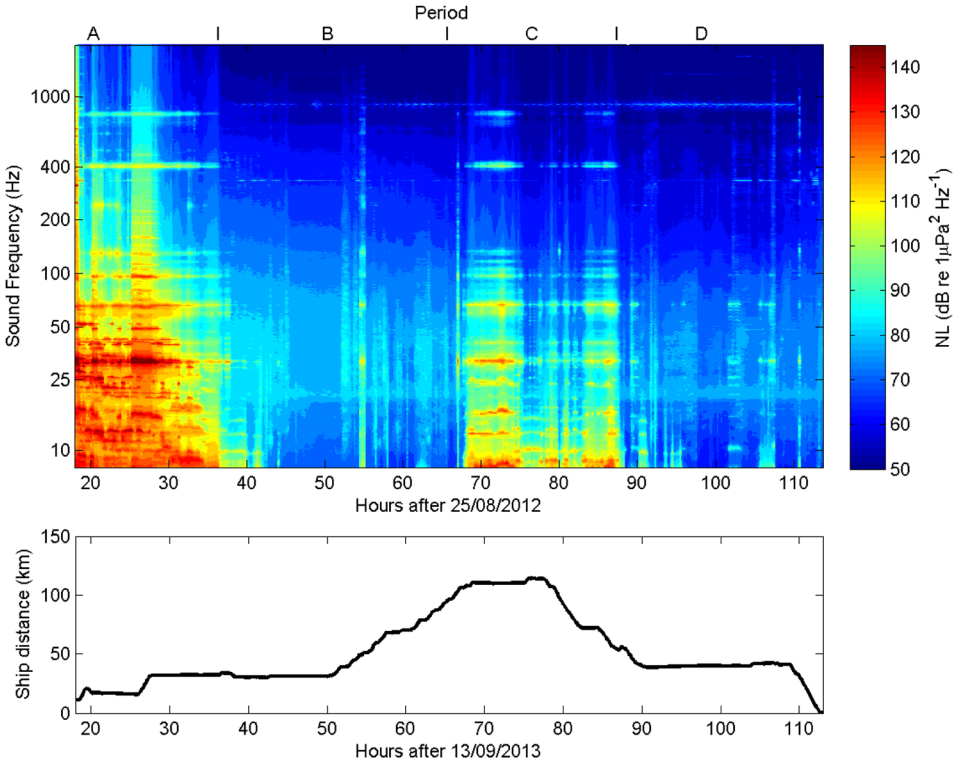

FIG. 3. (Color online) Overview of passive acoustic recording in the 2013 experiment. Upper panel: Spectrogram of 15-min mean acoustic NLs with 0.24 Hz frequency resolution. Four distinct periods are designated (A: hours 19–37, B: 40–67, C: 68–88, D: 89–111). Lower panel: Distance from icebreaker.

cavitation. Most striking is the strong overall increase in NLs for the middle (50%) to high percentile curves (90%). At the 90th percentile, NLs exceed 100 dB for frequencies up to 100 Hz. The 90th percentile curve also displays a large number of wide spectral peaks connected to ship screw cavitation during icebreaking activity, with the most prominent at 30, 75, 90, 400, and 800 Hz. Normal ship engine noise is visible as much narrower spectral peaks at 330 and 670 Hz in the 50th percentile curve. The strong peak at 900 Hz in the lower percentile curves stems from the acoustic communication experiment. In the lower percentile curves there is a wide spectral peak at 18–25 Hz. This was identified as the effect of fin whale vocalizations, which were much more common in 2013 than in 2012. Noises from other marine mammals were less frequent in 2013 than in the previous year and had hardly any impact on the overall soundscape.

Using spectrograms and NL distributions as a sound identification tool has limitations. Seismic airgun signals occur as a series of repeated shots with constant time intervals of 8–13 s for a typical duration of 30 min to two hours. This regular repetition pattern can be used to identify seismic airgun noise and quantify its contribution to the soundscape.

III. SEISMIC AIRGUN NOISE

Many man-made noises are either noises occurring at a constant frequency, e.g., the engine noise from a ship travelling at constant speed, or regularly pulsating noises, such as a series of seismic airgun shots. Airgun shots occur typically every 8–15 s, depending on the purpose of the seismic survey and the water depth in which the seismic exploration vessel is operating. This characteristic regularity of seismic airgun noise can be used to detect this type of noise and to separate and quantify its contribution to the observed soundscape. For this purpose a spectral analysis of the acoustic spectrograms was carried out.

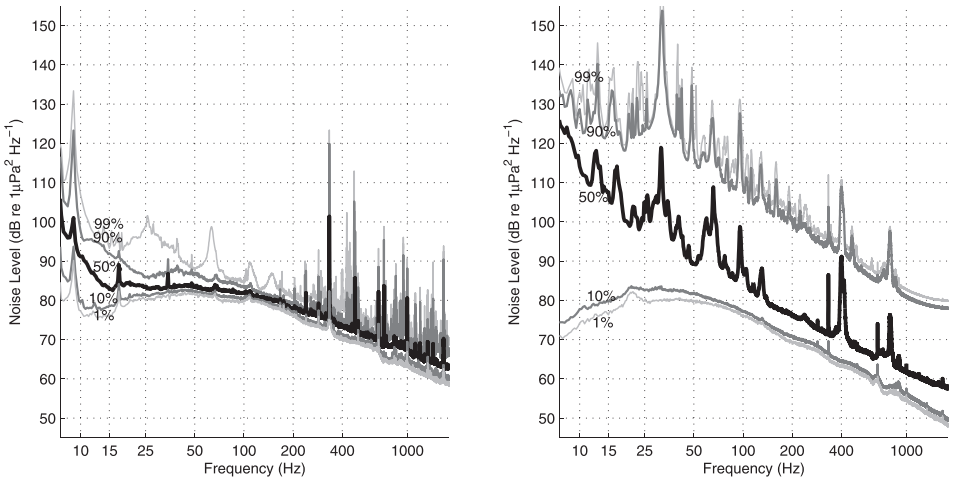

FIG. 4. Comparison of NL distributions of hourly mean NLs in the 2012 (left panel) and 2013 (right panel) experiments. 1, 10, 50, 90, and 99 percentiles are plotted with a frequency resolution of 0.24 Hz.

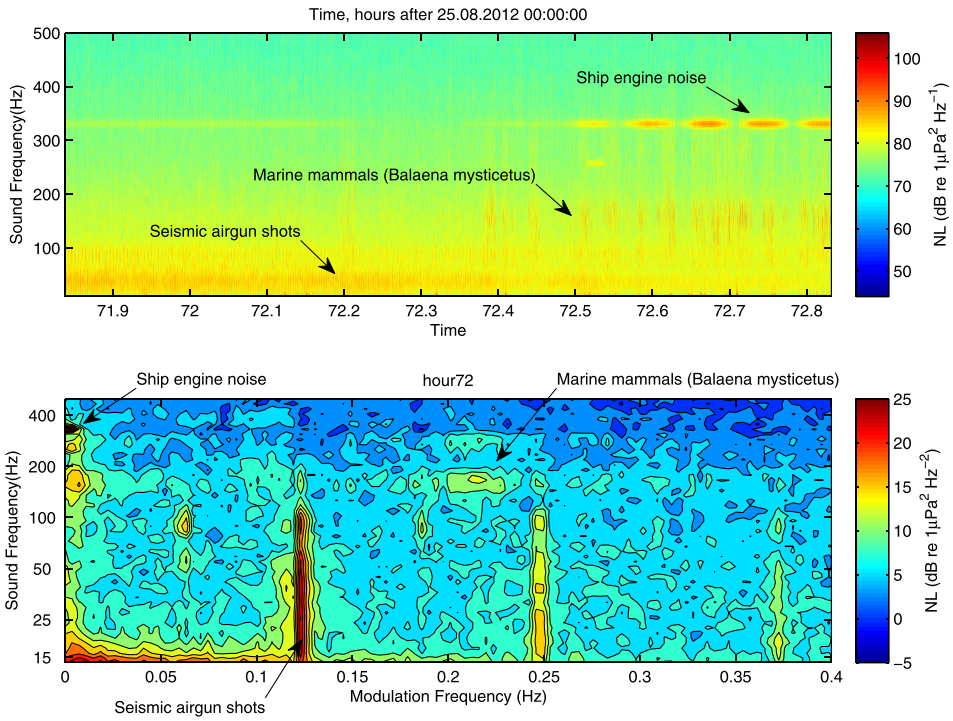

FIG. 5. (Color online) Upper panel: Spectrogram example (1 h duration) from the 2012 experiment displaying three annotated soundscape components: seismic airgun noise (50–100 Hz), marine mammal vocalizations (80–500 Hz), and ship noise (330 Hz). Lower panel: Power spectrum of the upper panel spectrogram, sound frequency along the y axis, frequency of sound amplitude modulation along the x axis. Three soundscape components are annotated: seismic airgun (15–100 Hz sound frequency, 0.12, 0.24, and 0.36 Hz modulation frequency), marine mammal noise (weak horizontal bands at 80–400 Hz sound frequency), and ship engine noise (330 Hz sound frequency, close to 0 Hz modulation frequency).

Acoustic spectrograms consist of time series of sound levels as a function of frequency. The spectrograms used here to study seismic airgun noise have a frequency resolution of 3.81 Hz and a time resolution of 0.131 s. For the following analysis the data were binned into 1/10 octave frequency bands to reduce the amount of data. Power spectra are then calculated for time series at each sound frequency for hourly recording intervals, averaging over 50% overlapping (detrended) Kaiser windows with a window length of 2048 samples. The new power spectra are a function of frequency bands (sound frequency) and modulation frequency, which describes the amplitude modulation of sound at a given frequency band. The power spectra can be presented as contour plots as shown in the lower panel of Fig. 5. The modulation frequency describes the variability of sound levels at a given frequency with time and can be used to identify sounds with a periodic pattern (e.g., repeated airgun shots). A continuous wave sound (e.g., ship engine noise) will have a modulation frequency close to 0 Hz.

Figure 5 (upper panel) presents an example of a spectrogram of one-hour duration. The spectrogram contains seismic airgun noise, marine mammal vocalizations, and ship engine noise. The different noise types are marked in the spectrogram. The lower panel of Fig. 5 shows the resulting power spectrum of the spectrogram. Natural sounds, such as marine mammal noises (in this case *Balaena mysticetus* calls), with their irregular time variation form wide horizontal bands. Seismic airgun noise is visible as vertical bars at 15–110 Hz acoustic frequency. The bar with the lowest modulation frequency identifies the shooting interval of the seismic exploration, while bars at higher modulation frequencies represent the harmonics. Ship engine noise with its slowly varying amplitude and narrow frequency band is observed as a point at 330 Hz sound frequency close to 0 Hz modulation frequency. The weak marine mammal noises in this example are visible as horizontal bands of increased power at 130–300 Hz acoustic frequency. Figure 5 shows an example with strong seismic noise and weak marine mammal noises. In the opposite case of strong marine mammal noise and weak seismic noise, the horizontal bands from the marine mammal noise would dominate, but the seismic signal would still be clearly identifiable due to its sharp signature in modulation frequency stemming from the precise timing of the repeating seismic airgun shots.

Power spectral densities of hourly spectrograms are calculated for the 2012 and 2013 experiments using a window length of 2048 samples as described above. Inspecting the power spectra shows seismic noise as a clear peak at modulation frequencies between 8–13 s (the repetition time of successive airgun shots) at sound frequencies of 15–120 Hz. The strongest signal occurs at 40 Hz sound frequency. An overview of the hourly power spectra of the 40 Hz noise time series during the 2012 experiment is shown in the upper panel of Fig. 6 for the typical modulation periods of the seismic airgun shots. The plot displays the noise component occurring at 40 Hz sound frequency and amplitude modulation periods of 7–15 s. This amplitude modulation period corresponds to the repetition times of the airgun shots. All peaks between 8 and 13 s in the upper panel of Fig. 6 were verified by listening to correspond to seismic airgun noise. Seismic airgun noise is present in 69 h out of 92 h total observation period in the 2012 experiment.

The analysis presented here allows the detection of even weak seismic signals and the precise determination of the sound frequencies influenced by the seismic airgun noise. Directly using the regular shooting intervals that characterize seismic airgun noise gives a high signal-to-noise ratio for seismic airgun noise vs the other noise contributing to the soundscape at the same sound frequencies as the seismic airgun noise. This motivates an attempt to construct a proxy

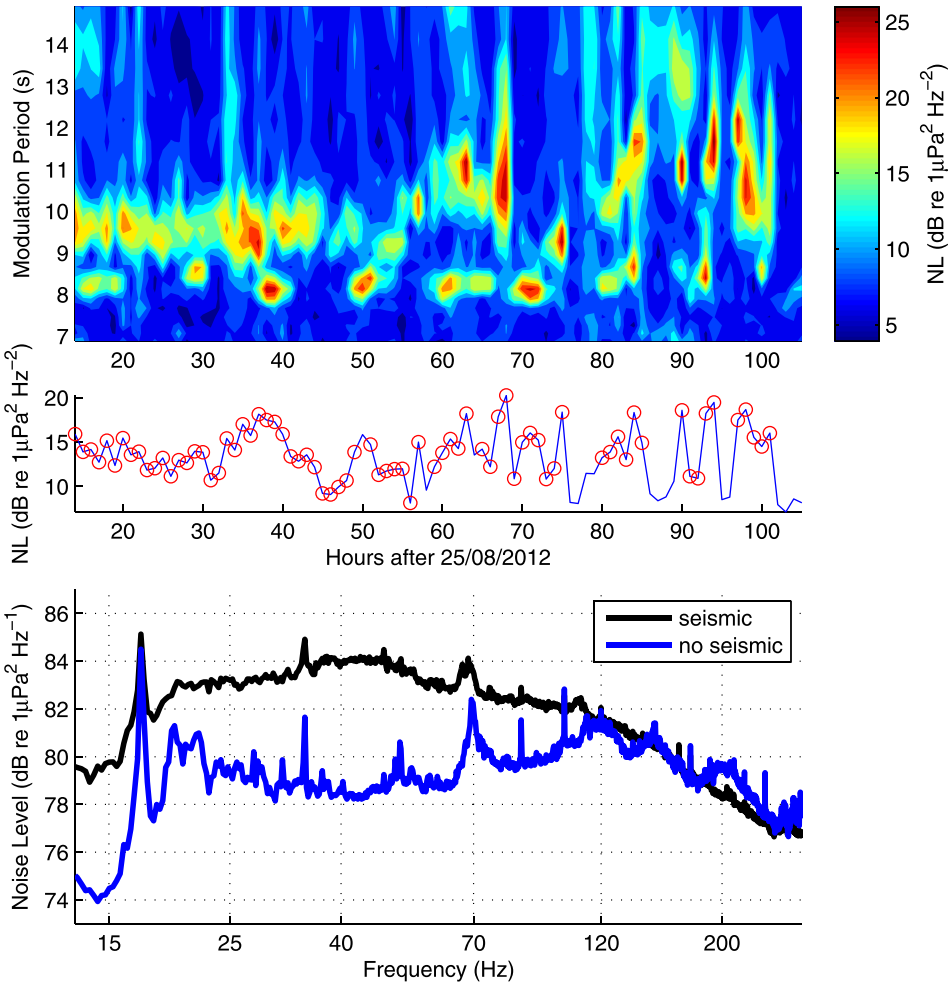

FIG. 6. (Color online) Upper panel: Overview of the power spectra of the 40 Hz noise time series for the 2012 experiment, zooming in on the amplitude modulation periods of seismic airgun noise. All peaks between 8–13 s modulation period were manually identified as seismic airgun noise. Middle panel: Proxy for seismic airgun noise—time series of mean power spectral densities of 40 Hz noise with 8–13 s amplitude modulation periods. Manually identified instances with seismic airgun noise are marked by circles. Lower panel: Comparison of NLs for periods with and without seismic airgun noise during the 2012 experiment. 50-percentile hourly mean NLs are plotted for both cases. Four hours with exceptionally strong contributions from other sound sources, such as ship maneuvering, ice breaking, and transient hydrophone noises, were excluded from the compared periods.

value for seismic airgun noise that could be used to automatically detect the presence of seismic airgun noise in longer time series. This proxy time series is calculated as the mean power density for the 8–13 s amplitude modulation band at 40 Hz sound frequency and is shown in the middle panel of Fig. 6. The proxy time series is tested against the manual identification of seismic exploration noise in the middle panel of Fig. 6. Hours with manually identified seismic exploration noise are marked by circles. The proxy time series compares relatively well to the manually identified occurrence of seismic noise. However, varying background levels mean that the correspondence is not perfect. Depending on the threshold chosen, there are 3–4 misses and 1–2 false detections out of 69 instances of seismic noise. The misses occur for the weakest identified seismic noise signals.

Using the manual detection of seismic airgun noise, the mean effect on low-frequency NLs is estimated. The lower panel of Fig. 6 shows the comparison of sound levels for periods with seismic airgun noise to periods without seismic airgun noise during the 2012 experiment. Five hours with exceptionally strong contributions from other sound sources, such as ship maneuvering and icebreaking, were excluded from this comparison. The presence of seismic exploration noise increases the low-frequency NLs between 20 and 120 Hz. The sound level increase due to seismic exploration noise is largest at 40–45 Hz, where the 50th percentile sound level of hourly data increased from 78 to 84 dB. At 100 Hz the NL increase caused by seismic exploration noise is still 2 dB at the 50th percentile. Differences below 20 Hz are caused by variable ship noise from icebreaking, as are the spectral peaks at 17, 34, 69, and 110 Hz. The comparison shows that seismic airgun noise causes a strong NL increase at low frequencies without forming a distinct spectral peak. This highlights the necessity of using the repetitive nature of seismic airgun shot series to identify and quantify this important component of the MIZ soundscape.

During the 2013 experiment large parts of the recordings were characterized by strong ship cavitation noise due to heavy icebreaking carried out by the research vessel (see Sec. IV). However, seismic noise is still an important part of the soundscape in the 2013 observations. The method introduced above was used to identify the seismic airgun noise in the same way as was done for the 2012 experiment. Seismic airgun noise was similar to that in 2012, with modulation periods of 8–15 s at sound frequencies between 15 and 150 Hz. Seismic noise was present in 48 out of 96 total observation hours, i.e., exactly half of the observation period. It is likely that the prevalence of seismic airgun noise was underestimated in 2013, as the extremely strong cavitation noise during periods A (hours 19–37) and C (hours 68–88, see Fig. 3) might have masked the presence of seismic airgun shots. Seismic airgun noise was present for practically all of the quiet periods B and D. The cavitation noise periods

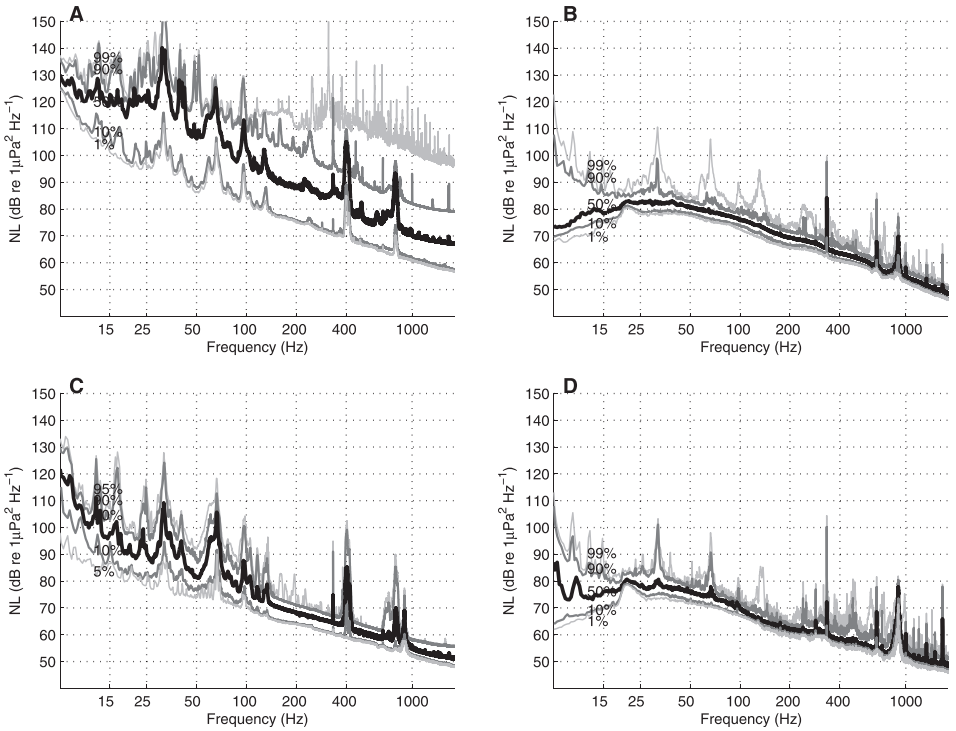

FIG. 7. Comparison of NLs distributions for four different periods in the 2013 experiment: (A) cavitation noise from nearby icebreaker, hours 19–37. (B) calm conditions, hours 40–67. (C) cavitation noise from distant icebreaker, hours 68–88. (D) normal ship activity, hours 89–111. 1, 10, 50, 90, and 99 percentiles are plotted. The peak at 900 Hz during periods B and D originates from an acoustic communication experiment carried out in parallel to the observations and is ignored in this analysis.

also influence the proxy for seismic exploration noise developed for the 2012 experiment. The increased background noise values during periods of strong cavitation noise would lead to numerous false detections if using the proxy for the 2013 data set. Therefore, this proxy cannot be used in the presence of very strong low-frequency ship noise. For the automatic analysis of longer time series, one would thus need to exclude such periods before carrying out the analysis.

IV. SHIP CAVITATION DURING ICEBREAKING ACTIVITY

Normal ship engine noise from a distant single ship influences only a small part of the underwater noise spectrum. Such noise was observed during large parts of the 2012 experiment as sharp spectral peaks at 330 and 600 Hz. The absolute NLs at the two spectral peaks were 96 and 80 dB, respectively, at the 50th percentile level (Fig. 4, left panel). During the "quiet periods" (periods B + D) of the 2013 experiment, the same spectral peaks were observed (Fig. 4, right panel).

In the 2013 experiment a much stronger type of noise was observed during periods A and C, raising the NLs by 20 dB and more over the entire observed sound spectrum (5–1950 Hz, Fig. 4, right panel). This dominant sound source was confirmed to be cavitation noise from heavy icebreaking activity of the research vessel by comparison with the ship position log and the detailed description of cavitation noise in the recent paper of Roth *et al.* (2013). The ship cavitation noise was strongest during backing-and-ramming maneuvers of the icebreaker during attempts to break through pressure ridges. Backing-and-ramming maneuvers were also identified as the source of the strongest instances of cavitation noise by Roth *et al.* (2013).

In addition to the broad spectral NL increase that ranges from more than 35 dB at 15 Hz to 20 dB at 1800 Hz, the ship cavitation noise was characterized by three low-frequency spectral peaks at about 30, 70, and 95 Hz and two high-frequency spectral peaks at 400 and 800 Hz (Fig. 4, right panel). The 400 and 800 Hz peaks are a characteristic ringing noise with an amplitude modulation frequency of about 4.5 Hz. To analyze the increase of sound levels due to cavitation noise, the time series was split into four parts (see Fig. 3). Period A, at hours 19–37, was dominated by cavitation noise from the icebreaker, which was 26 ± 7 km from the IIS, with a minimum distance of 15 km and a maximum distance of 34 km. During period B (hours 40–67), little cavitation noise was present. Period C (hours 68–88) was again dominated by cavitation noise, with the icebreaker 92 ± 22 km from the IIS. The minimum distance during this period was 45 km, and the maximum distance was 114 km. Cavitation noise was absent during period D (hours 89–111). A comparison of the two periods with cavitation noise (A, C) and the two periods without cavitation noise (B, D) can be seen in Fig. 7. During period A, with the icebreaker close by, NLs at the 30 Hz peak of the cavitation noise increased by more than 50 dB at the 50th percentile level, compared to the quiet periods. The whole noise spectrum up to 1000 Hz was elevated by at least 25 dB at the 50th percentile level. During period C, with cavitation noise from the distant icebreaker, the increase in sound level at 15 Hz was still as high as 28 dB at the 50th percentile level. Even at these distances, the whole noise spectrum up to 1000 Hz was elevated by 10 dB at the 50th percentile level.

During the 2012 experiment ship cavitation noise was only occasionally observed, as the ship was not engaged in heavy icebreaking comparable to the activities during the 2013 experiment. In the left panel of Fig. 4 the typical wide cavitation peaks at 30, 70, and 95 Hz are visible in the highest percentiles. None of the higher frequency cavitation

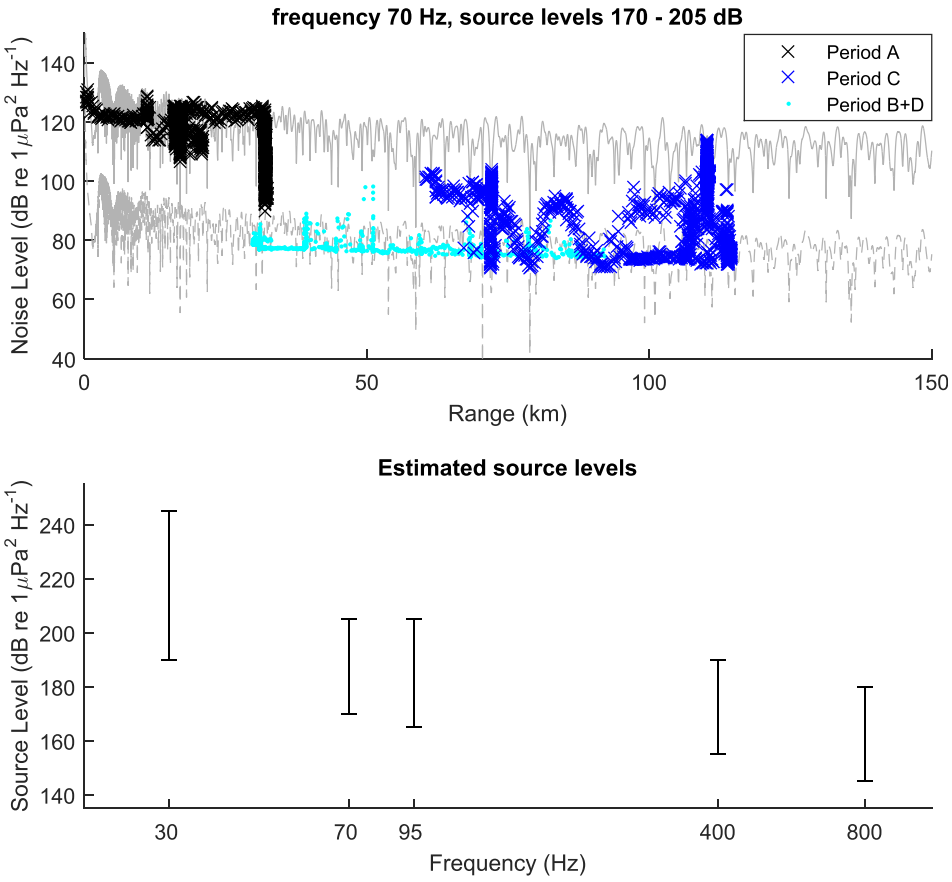

FIG. 8. (Color online) Upper panel: Cavitation noise versus range for the 70 Hz cavitation noise peak frequency. Separate periods are as defined in Sec. II: Close-by cavitation (period A), far-off cavitation (period C), quiet periods (periods B+D). Grey curves denote the modelled NL curves for the source levels of 205 dB (maximum estimate) and 170 dB (minimum estimate), forming upper and lower bounds for the cavitation noise. Lower panel: Estimated source level ranges for the five main frequency peaks of cavitation noise using the modelled transmission loss. Model setup: Source depth 6.5 m, ocean depth 2000 m, elastic sea-ice layer thickness: 2 m, sea ice density 0.9 km/dm,^{3} compressional wave speed 3600 m/s (attenuation 0.216 dB/Λ), shear wave speed 1800 m/s (attenuation 0.648 dB/Λ) following Laible and Rajan (1996).

peaks were observed in 2012. Other, less distinct icebreaking noises were observed at 10–25 Hz (90th percentile, Fig. 4, left panel). Icebreaking noises of this type were present on 29 out 92 total observation hours. The research vessel was always closer than 100 km from the integrated ice station during the 2012 experiment.

Strong cavitation noise during icebreaking activity in 2013 was measured at different distances from the ship. The NLs are compared to simulated levels from OASES (Ocean Acoustics and Seismic Exploration Synthesis model; Schmidt and Jensen, 1985). The model setup and results are found in Fig. 8. The horizontally constant sound-speed profile employed in the model was constructed using XCTD and XBT measurements carried out during the experiment. Roth *et al.* (2013) used an extensive set of measurements at a short distance from an icebreaker to calculate accurate source level. In our case the measurements were made at a substantial distance from the icebreaker. Correspondingly, we do not aim to calculate accurate source levels, but to establish the wide range of source levels produced by an icebreaker operating under varying (but heavy) ice conditions. This justifies the simplifications employed in the model calculation of sound propagation.

Figure 8 (upper panel) compares the measured NLs at 70 Hz as a function of the distance of the ship from the acoustic recorder with transmission loss calculations (in grey) using the OASES model for two source levels. The crosses refer to periods with cavitation noise, both with the ship nearby (period A) and at larger distance (period C), dots mark the quiet periods (periods B + D), when hardly any cavitation noise was observed (see Fig. 3 for the definitions of the periods). The cavitation noise events stand out above the background NL of 80 dB observed during the quiet periods without heavy icebreaking, allowing a clear identification of the cavitation noise. Using the modelled transmission loss as a function of distance, upper and lower source level bounds were estimated by fitting the model results (grey curves) to the observed NLs for each frequency (Fig. 8, upper panel). The lower bound refers to the lowest NLs still distinguishable from the background noise at the observed distances from the icebreaker. Similarly, the maximum and minimum source levels were calculated for the spectral peaks at 30, 95, 400, and 800 Hz. An overview of the source level estimates for the five frequency peaks is shown in the lower panel of Fig. 8. The estimates for the maximum source level range from 245 dB (30 Hz) to 180 dB (800 Hz).

Although these are rough estimates, higher source levels of cavitation noise were observed during heavy icebreaking than those reported by Roth *et al.* (2013). The main importance of these observations lies in the documentation of the strength of icebreaker cavitation noise at substantial distances from the icebreaking vessel and in the use of ship distance information to separate the cavitation noise from the constant background NLs, which are independent of ship distance (Fig. 8, upper panel).

V. MARINE MAMMALS

Marine mammal vocalizations were present during large parts of the 2012 and 2013 experiments. The NLs produced

by marine mammal vocalizations were lower than the seismic airgun NLs or the ship cavitation noise. They were, however, still an important part of the soundscape, increasing the NLs and especially the short-term NL variance around 20 Hz and between 100 and 500 Hz.

During the 2012 experiment the dominant marine mammal vocalizations were identified as bowhead whale (*Balaena mysticetus*) calls. The spectrogram in the upper panel of Fig. 5 shows such bowhead calls. The bowhead whale calls were present during 48 out of 92 observation hours. As the marine mammal vocalizations were weaker than the seismic airgun noise during the experiment, it was difficult to estimate the exact contribution of marine mammal vocalizations to mean sound levels. A maximum contribution was estimated by comparing hours before and after a sudden onset of strong marine mammal vocalizations and otherwise calm conditions, i.e., minimal disturbance from other soundscape components. Comparison of these subsequent hours with strongly differing marine mammal activity showed NL increases of 2–5 dB at several wide spectral peaks at 100–150, 200, and 390 Hz, with the strongest increases occurring at 120 Hz. In addition, a wider spectral range of about 80–1000 Hz shows slightly increased NLs during periods of strong marine mammal activity. During the 2013 experiment bowhead calls were absent. Several types of high frequency calls were instead observed, including sperm whale (*Physeter macrocephalus*) and narwhal (*Monodon monoceros*) vocalizations. They did not strongly influence hourly mean sound levels.

Fin whale (*Balaenoptera physalus*) vocalizations formed the marine mammal contribution to the low-frequency end of the soundscape during both the 2012 and 2013 experiments. Fin whale vocalizations could be identified during 9 out of 92 h in the 2012 experiment, with 1–5 vocalization sequences per hour. The vocalization sequences lasted about 10 min each with a call occurring about every 12 s. During the 2013 experiment, fin whale vocalizations were present during 24 out of 94 observation hours, a much higher percentage than in 2012. The vocalizations did not occur in distinct vocalization sequences in 2013, but as a continuous series of calls occurring roughly every 12 s for up to several hours. The maximum contribution from fin whale vocalizations was again estimated by comparing hourly mean NLs from subsequent hours with and without fin whale vocalizations during otherwise calm conditions. Fin whale vocalizations increased the mean hourly NLs by up to 10 dB at frequencies between 18 and 25 Hz.

VI. BACKGROUND NOISE

In this section we focus on the component of the soundscape related to the natural sound generating mechanisms and the sound propagation characteristics in the Arctic. Revisiting Fig. 4 we see that the shape of 1% and 10%

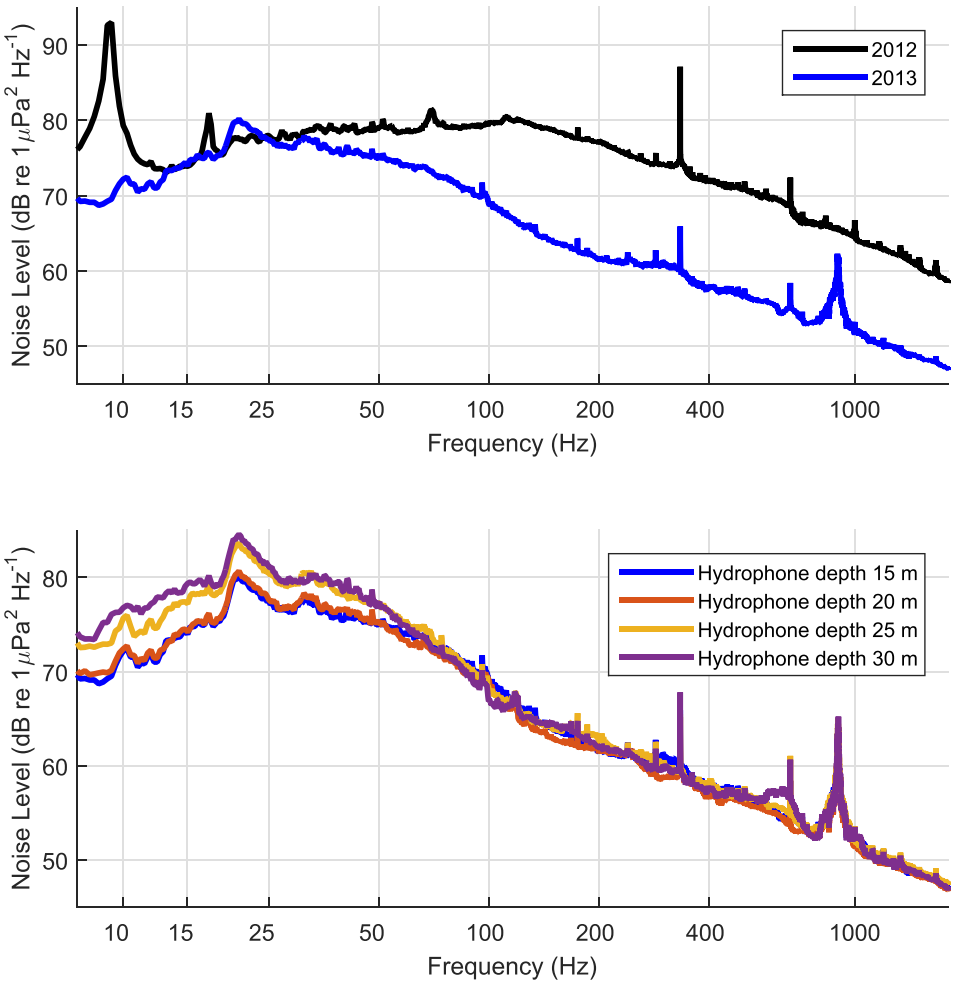

FIG. 9. (Color online) Upper panel: comparison of NLs during quiet periods in the 2012 and 2013 experiments. The 10th-percentile level is plotted for 2012 and 2013. Lower panel: comparison of 10th-percentile level noise at different depths in 2013.

percentiles are similar to each other, and their smoothness indicates a minimum influence from ship cavitation noise and other transient noise events, such as seismic noise and marine mammals. We therefore claim that 1% and 10% percentiles represent the background NL caused by the natural environment even in the presence of very loud anthropogenic noise during substantial parts of the acoustic record. Remaining non-natural noise signatures in Fig. 9 are peaks related to strumming (9 Hz, 2012), ship engine noise (330, 660 Hz), and noise from an underwater communication experiment (900 Hz, 2013). Those noise signatures in the 10th-percentile NLs are narrowband and do not impact the analysis of the natural background noise below.

The 10th-percentile NLs in 2012 and 2013 are compared in the upper panel of Fig. 9. A logarithmic decay of NLs with frequencies is observed above 50 Hz in 2013 and above 100 Hz in 2012. The logarithmic decay with frequency is typical in the MIZ and is established by the Arctic propagation conditions (e.g., Buckingham and Cheng, 1988; Sagen, 1998; Johannessen *et al.*, 2003). Furthermore, we observe that the NL in 2012 was higher than in 2013. The difference in NL increased gradually from being equal at 30 Hz to 12 dB at 200 Hz. Above 200 Hz the difference was constant up to 1800 Hz.

Table I shows that in 2012 the compact ice edge was combined with moderate (1 m) to strong (2 m) wave conditions and strong inertial oscillations. In 2013 the ice edge was compact as well, but the wave measurements showed weak swell conditions. In 2013 the IIS was located approximately 15 km further into the ice pack from the ice edge than in 2012. While the absolute wind speeds during the 2012 and 2013 experiments were comparable, the wind directions were different. The prevalent south-easterly wind in 2012 led to a strong compression of the ice edge (Fig. 1), as opposed to the steady northerly wind in 2013, which neither compressed nor spread the ice. Also in 2012, waves-on-ice conditions were observed with larger wave heights than in 2013 as measured by the integrated ice station's wave-in-ice buoy (see Sec. II). We therefore conclude that the 12 dB higher NLs observed in 2012 compared to 2013 can be explained by the different positions of the IIS with respect to the ice edge and by differences in wind, wave, and ice conditions. Similar relation of then NLs to the distance to ice edge and wave conditions has been reported by Johannessen *et al.* (2003).

Table II compares the ambient NLs observed in this study with earlier experiments. The different environmental conditions are given for the various experiments. The comparison shows that at 315 Hz the highest levels are found at the compact ice edge (78–79 dB), intermediate levels a few kilometres into the ice pack (75 dB), and that the lowest levels are found well into the ice edge (61 dB). A similar reduction of ambient NLs in to the ice pack is observed at 1000 Hz.

The strong relation between observed NLs and distance into the ice pack from a compact ice edge is well known (e.g., Diachok and Winokur, 1974; Yang *et al.*, 1987; Johannessen *et al.*, 2003). Swell and wind generated waves interacting with a compact ice edge produce many sound generating events such as floe-floe interaction, and increased wave breaking just outside the ice edge. This increases the ambient NL at the ice edge. The short wind-generated waves dampen rapidly down and do not propagate far into the ice pack, while the long waves (swell) are attenuated much slower while propagating into the ice pack. Therefore, in the case of a compact ice edge and swell, the sound generation caused by swell will gradually be reduced with distance into the ice pack. In the case of off-ice wind conditions or low winds in a very dynamic area a diffuse ice edge will result. In such cases the NLs in the MIZ are more variable and less related to the distance from the ice edge (Johannessen *et al.*, 2003). In diffuse ice edges the high NLs are related to convergence zones due to ice edge eddies, and low levels are related to areas with grease ice and new frozen ice (Johannessen *et al.*, 2003).

The ambient noise field is composed by contribution from a large number of distant and nearby sources, and therefore flavoured by the acoustic propagating conditions. In general, the low-frequency ambient noise is dominated by distant sources, while the higher frequency components correspond to nearby sources (e.g., Buckingham and Cheng, 1988). The lower panel of Fig. 9 displays the 10th percentile NLs at four different hydrophone depths between 15 m and 30 m. Low-frequency noise ($f < 50$ Hz) shows a clear depth dependency with NLs increasing by 3–5.5 dB from 15 to 30 m depth. No depth dependence is observed for frequencies above 70 Hz. Long-range transmission loss estimates at 100–150 km source range calculated with the OASES

TABLE II. Comparison of median ambient NLs to earlier NL measurements in the Fram Strait MIZ. All NLs are in dB re 1 μPa^2/Hz. For the WIFAR 2013 experiment only period D (see Fig. 3) is displayed to minimize ship influence.

Frequency	315 Hz	1000 Hz	Distance from ice edge [km]	Ice conditions	Wind and wave condition
WIFAR 2012	75	67	5.2–6.3	Compact ice	On-ice wind: 2–10 m/s Swell: 0.25–1.9 m significant wave height
WIFAR 2013, period D	61	53	20.8	Compact ice	Along ice-edge wind: 2–4 m/s, No swell: 0.25 m significant wave height
Diachok and Winokur, 1974	79	68	0	Compact ice edge	Sea state: 2
Yang *et al.*, 1987	78	—	0	Compact ice edge	Sea state: 2
MIZEX 1987, Johannessen *et al.*, 2003	78	68-69.5	1.0–10.0	Compact ice edge	Wind: 5–9 m/s parallel to ice edge Swell: 0.7–1.5 m significant wave height
MIZEX 1985, Johannessen *et al.*, 2003	70.7	63.5	1.0–35.0	Diffuse ice with eddies	Wind: 3-5 m/s parallel to ice edge No swell: <0.5 m significant wave height
Yang *et al.*, 1987	64	—	0	Diffuse ice edge	Sea state: 2

TABLE III. Comparison of NL changes due to different soundscape components.

Sound component	Mean NL increase	Frequency range
Seismic airgun noise (distance > 800 km)	2–6 dB	$f = 20$–120 Hz
Ship cavitation noise	28 dB	$f = 15$ Hz
(≈100 km distance)	>10 dB	$f < 1000$ Hz
Marine mammal vocalizations	<10 dB[a]	$f = 18$–25 Hz (fin whale)
	<5 dB[a]	$f = 100$–400 Hz (bowhead whale)
Background noise	12 dB	$f > 100$ Hz

[a]Maximum estimates.

simulation described in Sec. IV yield a mean noise increase with depth of 5.6 dB at 30 Hz frequency and an increase of 3.1 dB at 70 Hz frequency. No depth dependency is observed at 400 Hz frequency. The observed and modelled depth dependency is in accordance with mode theory as the main energy for low frequencies is in the lower modes, which have a maximum at 80–100 m depth. For a 150 m thick surface duct with a sound speed of 1440 m/s the estimated cutoff frequency is around 100 Hz. Above this frequency the acoustic energy is trapped in the surface channel underneath the sea ice. This leads to vertical uniform distribution of the acoustic energy with in the surface channel. Furthermore, the ducted acoustic energy repeatedly interacts with the sea ice leading to the characteristic f-n dependency in the frequency spectrum (e.g., Buckingham and Cheng, 1988; Sagen, 1998).

VII. CONCLUSIONS

It was possible to separate and quantify the four major components of MIZ soundscape as measured by the experiments carried out in 2012 and 2013. Seismic airgun noise, ship cavitation, and the variations of the natural background noise due to differing geophysical conditions were all substantial contributors to shaping the soundscape variability during the two four-day experiments. To a lesser degree, the frequent marine mammal vocalizations also played a part in shaping the observed noise spectra in the MIZ. Table III gives an overview of the observed mean NL changes due to different sound sources.

In this study ship cavitation caused by heavy icebreaking is the dominant source, increasing the NL by more than 10 dB below 1000 Hz and 28 dB at 15 Hz (Table III). The cavitation noise during the 2013 experiment dominates at distances as large as 100 km from the icebreaker. This implies that this type of noise may change the Arctic soundscape significantly, in particular, with the expected increase of icebreaker activity in the Arctic. Furthermore, this study shows that sound production during icebreaker operations in the MIZ depends strongly on how heavy the ice conditions are, and suggests that choosing routes, which minimize heavy icebreaking, will reduce the noise contribution from icebreakers. Little is known about the prevalence of cavitation noise in the Arctic and the cumulative effect of increased icebreaker activity on the Arctic soundscape. Analysis of longer time series would provide information on how common this type of ship noise is in the Fram Strait MIZ.

The background noise generated by natural processes is another strong contributor to NL variability in the MIZ. The dynamic conditions observed in the 2012 experiment raise the NL compared to the measurements in 2013 by 12 dB between 200 and 1800 Hz. Several publications have previously reported similar strong variability of natural sound levels in the MIZ due to the impact of swell propagating into the ice edge, depending on the compactness of the ice edge and the distance from the ice edge (e.g., Makris and Dyer, 1991; Bourke and Parsons, 1993; Sagen, 1998; Johannessen *et al.*, 2003; Sagen *et al.*, 2014).

The contribution of 2–6 dB from distant seismic airgun shots to NLs in the MIZ as observed in the 2012 and 2013 experiments was somewhat weaker than the first two soundscape components mentioned here (Table III). However, the prevalence of seismic airgun noise was remarkable. During the two experiments seismic airgun noise was observed during 117 h out of 188 observation hours. This is likely an underestimate due to extreme ship cavitation noise preventing the detection of seismic airgun noise during part of the 2013 experiment. The nearest operational area of seismic exploration vessels during the experiments was in the southwestern Barents Sea, at least 800 km from the experiment sites. Due to the large distance from the possible sound source, the measured airgun noise can be seen as representative for—and therefore highly relevant to—large parts of the MIZ of the European Arctic. Moore *et al.* (2012) have reported high prevalence of airgun signals in Fram Strait for large parts of the year. As seismic exploration might move further north in the future, monitoring such noise and further investigations on how fast it is attenuated with distance into the ice pack (see Tollefsen and Sagen, 2014; Tollefsen *et al.*, 2015) seems highly relevant. Due to its easily recognizable regular sequences of repeated shots, seismic airgun noise was also the soundscape component that showed the greatest promise for automated detection and quantification. The spectral analysis methods described in Sec. III form a possible basis for such a detection algorithm.

Bowhead whale, sperm whale, narwhal, and fin whale calls were identified in the acoustic recordings. The contributions of marine mammal vocalizations to the observed noise spectra were of second order compared to the other soundscape components during both the 2012 and 2013 experiments. It was therefore more difficult to quantify the mean contribution of marine mammals to the observed soundscape, and the maximum effect of the observed marine mammal vocalizations on hourly mean NLs was estimated instead. This was done by finding sudden onsets of strong marine mammal vocalizations during otherwise calm periods, i.e., periods with minimal disturbance from other soundscape components. A comparison of the hourly mean spectra before and after the onset of the marine mammal vocalizations was then used to determine the values presented in Table III. Marine mammal vocalizations, while mostly not very strong in terms of their contribution to mean NLs, were prevalent during large parts of the recording. Their complex

patterns often stand out on spectrograms of the acoustic record.

ACKNOWLEDGMENT

We first want to thank the Norwegian coast guard for providing ship time with the icebreaker KV Svalbard, and the crew on board KV Svalbard for excellent and enthusiastic support during the field experiments. We thank Kathleen J. Vigness-Raposa for helping to identify the marine mammal species in the recordings and Asuka Yamakawa for providing the geographic areas of seismic airgun operations during the experiments. Finally, Håkon Johan Sandven is acknowledged for his initial processing and analysis of the acoustic data during his summer job at NERSC. This work has been carried out under funding from the Research Council of Norway and GDF SUEZ through the WIFAR and UNDER ICE projects. The publication of this paper has been supported by the institutional basic funding from the Ministry of Climate and Environment.

Bourke, R. H., and Parsons, A. R. (**1993**). "Ambient noise characteristics of the northwestern Barents Sea," J. Acoust. Soc. Am. **94**(5), 2799–2808.

Buckingham, M. J., and Cheng, C. (**1988**). "Ambient noise in the Arctic Ocean below the Marginal Ice Zone," in *Natural Mechanisms of Surface Generated Noise in the Ocean*, edited by B. R. Kerman (Kluwer, Dordrecht, 1993), pp. 1–15.

de Steur, L., Hansen, E., Mauritzen, C., Beszczynska-Möller, A., and Fahrbach, E. (**2014**). "Impact of recirculation on the East Greenland Current in Fram Strait: Results from moored current meter measurements between 1997 and 2009," Deep-Sea Res. I **92**, 26–40.

Diachok, O. I., and Winokur, R. S. (**1974**). "Spatial variability of underwater ambient noise at the Arctic ice-water boundary," J. Acoust. Soc. Am. **55**, 750–753.

Freitag, L. (**2015**). (private communication).

Johannessen, O. M., Sagen, H., and Sandven, S. (**1994**). "The influence of grease ice, swell and icebergs on ambient noise," in *Proceedings of the Second European Conference on Underwater Acoustics*, edited by L. Bjørnø, European Commission Directorate-General XIII Telecommunications, Information Market and Exploitation of Research, Luxembourg, pp. 53–58.

Johannessen, O. M., Sagen, H., Sandven, S., and Stark, K. V. (**2003**). "Hotspots in ambient noise caused by ice-edge eddies in the Greenland and Barents seas," IEEE J. Oceanic Eng. **28**, 212–228.

Kinda, B. (**2013**). "Acoustic remote sensing of Arctic Sea ice from long term soundscape measurements, Signal and image processing," Ph.D. thesis, Université de Grenoble, Grenoble.

Klinck, H., Nieukirk, S. L., Mellinger, D. K., Klinck, K., Matsumoto, H., and Dziak, R. P. (**2012**). "Seasonal presence of cetaceans and ambient noise levels in polar waters of the North Atlantic," J. Acoust. Soc. Am. **132**, EL176–EL181.

Laible, H. A., and Rajan, S. D. (**1996**). "Temporal evolution of under ice reflectivity," J. Acoust. Soc. Am. **99**(2), 851–865.

Lewis, J. K., and Denner, W. W. (**1988**). "Arctic ambient noise in the Beaufort Sea: Seasonal relationships to sea ice kinematics," J. Acoust. Soc. Am. **83**(2), 549–565.

Lynch, J. F., Wu, H. X., Pawlowicz, R., Worcester, P., Keenan, R. E., Graber, H. C., Johannessen, O. M., Wadhams, P., and Schuchman. R. A. (**1993**). "Ambient noise measurements in the 200–300 Hz band from the Greenland Sea tomography experiment," J. Acoust. Soc. Am. **94**(2), 1015–1033.

Makris, N., and Dyer, I. (**1986**). "Environmental causes of pack ice noise," J. Acoust. Soc. Am. **79**(5), 1434–1440.

Makris, N. C., and Dyer, I. (**1991**). "Environmental correlates of Arctic ice edge noise," J. Acoust. Soc. Am. **90**, 3288–3298.

Moore, S. M., Stafford, K. M., Melling, H., Berchok, C., Wiig, Ø., Kovacs, K. M., Lydersen, C., and Richter-Menge, J. (**2012**). "Comparing marine mammal acoustic habitats in Atlantic and Pacific sectors of the High Arctic: Year-long records from Fram Strait and the Chukchi Plateau," Polar Biol. **35**, 475–480.

Pritchard, R. S. (**1990**). "Sea ice noise-generating processes," J. Acoust. Soc. Am. **88**, 2830–2842.

Roth, E. H., Schmidt, V., Hildebrand, J. A., and Wiggins, S. M. (**2013**). "Underwater radiated noise levels of a research icebreaker in the central Arctic Ocean," J. Acoust. Soc. Am. **133**(4), 1971–1980.

Sagen, H. (**1998**). "Ambient noise in the Marginal Ice Zone," Ph.D. thesis, University of Bergen, Bergen.

Sagen, H., Tollefsen, D., and Tengesdal, H. C. (**2014**). "The soundscape of the Fram Strait Marginal Ice Zone," in *UAC 2014-2nd International Conference and Exhibition on Underwater Acoustics*, Rhodes, Greece.

Schmidt, H., and Jensen, F. B. (**1985**). "A full wave solution for propagation in multilayered viscoelastic media with application to Gaussian beam reflection at fluid-solid interfaces," J. Acoust. Soc. Am. **77**, 813–825.

Tollefsen, D., Dombestein, E. M., and Sagen, H. (**2015**). "Modelling of noise due to distant seismic exploration in the Marginal Ice Zone," in *Proceedings of EuroNoise 2015*, Maastricht, the Netherlands, pp. 1383–1386.

Tollefsen, D., and Sagen, H. (**2014**). "Seismic exploration noise reduction in the Marginal Ice Zone," J. Acoust. Soc. Am. **136**(1), EL47–EL52.

Yang, T. C., Giellis, G. R., Votaw, C. W., and Diachok, O. I. (**1987**). "Acoustic properties of ice edge noise in the Greenland Sea," J. Acoust. Soc. Am. **82**, 1034–1038.